energies

Article

Thermodynamic Analysis and Optimization Design of a Molten Salt–Supercritical CO_2 Heat Exchanger

Xiaoming Dong, Cancan Zhang, Yuting Wu *, Yuanwei Lu and Chongfang Ma

MOE Key Laboratory of Enhanced Heat Transfer and Energy Conservation, Beijing Key Laboratory of Heat Transfer and Energy Conversion, Beijing University of Technology, Beijing 100124, China
* Correspondence: wuyuting@bjut.edu.cn

Abstract: The performance of a heat exchanger is directly related to the energy conversion efficiency of the thermal storage system, and its optimal design is an important method to improve the performance of the heat exchanger. This paper uses the distributed parameter method to analyze the effect of the structural parameters and operating parameters of a heat exchanger on the entransy dissipation rate, the entransy dissipation number, the entransy dissipation heat resistance, entropy production rate, and entropy production number in a molten salt–supercritical CO_2 concentric tube heat exchanger. The results show that the entransy dissipation rate and entropy production rate have the same trend, with the structural parameters and operating parameters, as well as the changes in the entransy dissipation number and entransy dissipation thermal resistance, jointly affected by the entransy dissipation rate and the heat exchange. Based on the above indicators, single-objective and multi-objective optimization calculations were carried out. The results show that taking the minimum entropy dissipation number, entransy dissipation heat resistance, and improved entropy production number as the objective functions, and using the heat transfer effectiveness as the evaluation index, the optimization effect is better. The ε value is increased by 41.2%, 39.5%, and 40.3% compared with the reference individual. In the multi-objective optimization, taking the minimum number of entransy dissipation and entropy production as the objective function, and using the efficiency of heat transfer and the pressure drop of the working fluid as the evaluation indicators, the optimization effect is better. Compared with the reference individual, the ε value increased by 23.5%, and ΔP_h and ΔP_c decreased by 51.9% and 32.5%, respectively. This study provides a reference for the optimization of supercritical CO_2 heat exchangers by utilizing parameters such as entransy and entropy, which reflect the irreversible loss of the heat transfer process.

Keywords: thermodynamic analysis; entransy dissipation; entropy dissipation; thermal storage system

check for updates

Citation: Dong, X.; Zhang, C.; Wu, Y.; Lu, Y.; Ma, C. Thermodynamic Analysis and Optimization Design of a Molten Salt–Supercritical CO_2 Heat Exchanger. *Energies* **2022**, *15*, 7398. https://doi.org/10.3390/en15197398

Academic Editor: Gabriela Huminic

Received: 6 September 2022
Accepted: 29 September 2022
Published: 9 October 2022

1. Introduction

Molten salt is one of the most promising heat transfer and energy storage medium, and the heat exchange between molten salt and supercritical CO_2(sCO_2) is of great significance for thermal storage system in solar thermal power generation [1,2]. Heat exchanger can realize the energy exchange between the hot and cold fluids, occupying a crucial position in the field of energy utilization, especially in the current background of energy conservation and emission reduction. So, it is particularly important to improve the efficiency of heat exchangers; subsequently, many studies were carried out to meet this demand [1,3]. On the one hand, new technologies, new theories, and new materials are applied to develop new heat exchangers, but there are disadvantages, such as the high cost and long cycle [3–5]. On the other hand, optimization design is carried out on the basis of existing heat exchanger to improve the efficiency of the heat exchanger, with the advantages of a short research period, low cost, quick effect, and so on [6,7].

The actual heat transfer process will lead to continuous attenuation of energy quality, namely, irreversible loss. Therefore, some scholars put forward the optimization rule of heat exchangers based on the second law of thermodynamics [6–8]. Bejan [7] et al. defined the dimensionless entropy production of heat exchangers and found that when the efficiency of a balanced-flow countercurrent heat exchanger is at 0.5, it will reach the maximum value, resulting in the entropy production paradox. To solve this problem, Hesselgreaves [8] and Ogiso [9] et al. proposed the improved form of entropy production to eliminate the paradox of entropy production. Shah [10] et al. analyzed the relationship between the efficiency of 18 different types of heat exchangers and the entropy production rate, and the results showed that when the entropy production rate was the lowest, the efficiency of the heat exchangers could be any value. In order to solve the problem of the entropy production paradox, Guo [11] et al. proposed the optimization criterion of a heat exchanger, the extremum principle of entransy dissipation, and the principle of minimum thermal resistance, based on the second law of thermodynamics. Guo [12] et al. proposed the entransy dissipation number and applied it to the evaluation of heat exchangers. Lerou [13] et al. analyzed the main causes of entropy generation of a heat exchanger in the cooling process, obtained a mathematical model for quantitative calculation of entropy generation, and carried out a structural optimization design by using the principle of minimum entropy generation. Chen [14] et al. proposed an entransy dissipation-based thermal-resistance method for an optimization design of heat exchangers, which could be more convenient for analysis and optimization. Wang [15] et al. optimized the wound tube heat exchanger based on the principle of minimum entransy dissipation thermal resistance. Guo [16] et al. optimized shell and tube heat exchangers with the entransy dissipation number and pressure entransy dissipation number as the objective function. Qian [17] et al. found that thermal resistance based on minimum entropy production does not always correspond to the highest heat transfer rate. Cheng [18] et al. analyzed the changes in entransy dissipation rate and entropy production rate with the change in heat exchanger working conditions, and found that the minimum entropy production rate and entransy dissipation rate does not always correspond to the best performance of the heat exchanger. Liu [19] et al. studied the applicability of the principle of minimum entropy production and the maximum principle of entransy in heat exchanger optimization. Guo [20] et al. established the principle of uniform distribution of entransy dissipation, and theoretically analyzed the application range of the principle of minimum entropy generation and the principle of extreme value of entransy dissipation. Xie [21] et al. carried out topology optimization on the needle-fin heat exchanger structure based on the principle of minimum entropy production, and the result showed that the heat storage of the system could be increased by 10.2%. Guo [22] et al. defined the dissipative thermal resistance of the heat exchanger based on the entransy dissipative thermal resistance and found that it has universality. Li [23] et al. optimized the design of serrated fins in plate-fin heat exchangers using the principle of minimum entransy dissipation heat resistance. Han [24] et al. optimized the structure of the new airfoil heat exchanger based on the idea of synergistic strengthening based on the distribution matching of entransy, and proposed two non-uniform fin distribution structures. Based on the exergy analysis of the coiled-tube heat exchanger, Han [25] et al. proposed the heat transfer exergy loss number, and used this dimensionless parameter to optimize the design of the coiled-tube heat exchanger. Although entropy theory and entransy theory have been used to study the optimization of heat exchangers, the influence of structural parameters and operating parameters on heat exchangers is rarely reported.

In this paper, the concentric tube heat exchanger is taken as the research object, molten salt and supercritical CO_2 are selected as the heat transfer medium, and the mathematical model is established by the distributed parameter method. The variation in the entransy dissipation rate, the entransy dissipation number, the entransy dissipation resistance, the entropy production rate, and the improved entropy production rate, with the structural parameters and operational parameters of a heat exchanger with a constant heat exchange surface and constant heat exchange, are analyzed. Based on the above parameters and heat transfer coefficient, single-objective optimization and multi-objective optimization calculations are carried out. Through this paper, by thermodynamic and optimization analysis of a supercritical CO_2 heat exchanger, on the one hand, we can reveal a change in the law of irreversible loss of the heat exchanger during operation and provide a certain reference for the design of a heat exchanger; on the other hand, we can provide guidance for the optimization of heat exchangers according to the optimization results.

2. The Computational Model and Model Validation

2.1. Physical Model and Heat Transfer Fluid

Figure 1 is the schematic diagram of concentric tube heat exchanger, and the inner diameter, outer diameter, and length are marked. The fluid in the tube is molten salt, and the fluid in the outer casing is supercritical CO_2. The inner diameter of the heat exchanger is 0.02 m, the outer diameter is 0.034 m, and the length is 2 m.

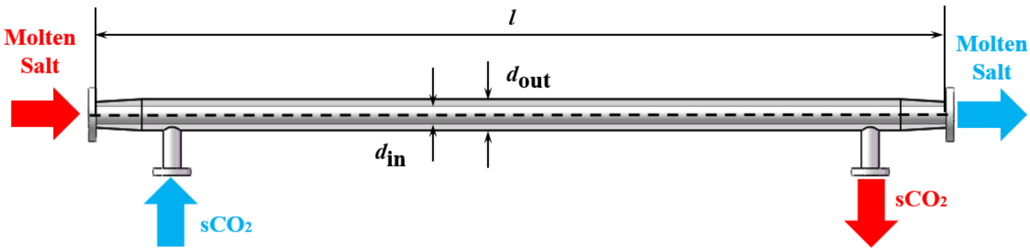

Figure 1. The schematic diagram of the concentric tube heat exchanger.

Figure 2 shows the thermal property parameters of molten salt and sCO_2, and ρ, c_p, λ, and μ represent density, specific heat capacity, thermal conductivity, and dynamic viscosity, respectively. The molten salt is self-configured mixed molten salt, and its thermophysical parameters are obtained through experimental test. For the sCO_2, its thermophysical parameters are obtained from NIST REPROP 9.0 [26] under the pressure condition of 8 MPa, with temperature range of 273–773 K.

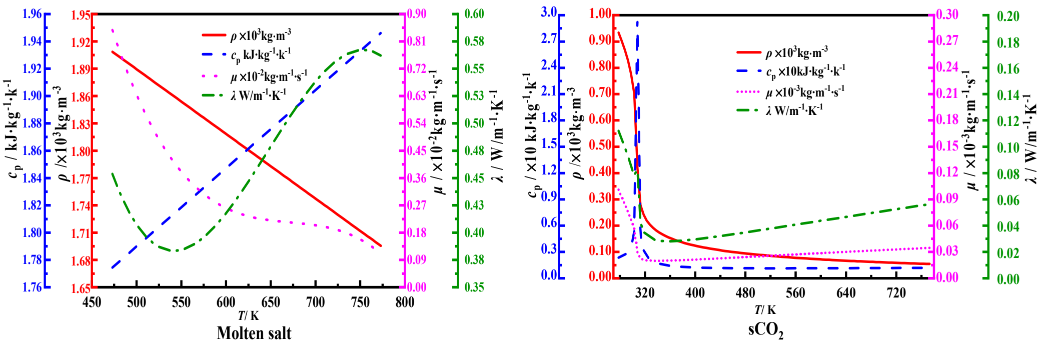

Figure 2. The thermal property parameters of molten salt and sCO_2.

2.2. The Computational Model

The concentric tube heat exchanger is divided into several units along the length, and the fluid was calculated as the steady state of one-dimensional flow, and the axial heat conduction of the inner wall was ignored, while the outer wall was adiabatic.

Continuity equation:

$$\frac{\partial(\rho u)}{\partial x} = 0 \tag{1}$$

where u is the velocity of the fluid, in m/s.

Momentum conservation equation:

$$\frac{\partial(\rho u^2)}{\partial x} + \frac{\partial P}{\partial x} + \frac{f u^2}{2D}\rho = 0 \tag{2}$$

where P is pressure, in Pa; and f is the resistance coefficient, which is calculated by Equation (3) [27]:

$$f = (1.82\log_{10}(Re) - 1.64)^{-2} \tag{3}$$

Energy conservation equation of the fluid in the tube:

$$A_{\mathrm{h}}\rho_{\mathrm{h}}c_{\mathrm{p,h}}u_{\mathrm{h}}\frac{\partial T_{\mathrm{h}}}{\partial x} = \alpha_{\mathrm{h}}(T_{\mathrm{h}} - T_{\mathrm{w}})\pi D \tag{4}$$

where A is the cross-sectional area, in m^2; α is the heat transfer coefficient, in $\mathrm{W{\cdot}m^{-2}{\cdot}K^{-1}}$; and D is the equivalent diameter, in m.

Energy conservation equation of outer pipe fluid:

$$A_{\mathrm{c}}\rho_{\mathrm{c}}c_{\mathrm{p,c}}u_{\mathrm{c}}\frac{\partial T_{\mathrm{c}}}{\partial x} = \alpha_{\mathrm{c}}(T_{\mathrm{w}} - T_{\mathrm{c}})\pi D \tag{5}$$

Energy equation of the wall:

$$\alpha_{\mathrm{h}}(T_{\mathrm{h}} - T_{\mathrm{w}}) = \alpha_{\mathrm{c}}(T_{\mathrm{w}} - T_{\mathrm{c}}) \tag{6}$$

The convective heat transfer of molten salt is calculated by the Gnielinski correlation [24]:

$$Nu = \frac{(f/8)(Re - 1000)Pr}{1 + 12.7\sqrt{f/8}\left(Pr^{\frac{2}{3}} - 1\right)} \tag{7}$$

where Nu is The Nusselt number and Pr is the Prandtl number.

The heat transfer coefficient of sCO_2 is calculated by using the local empirical correlation proposed by Jackson et al. [28]:

$$Nu = 0.0183Re^{0.82}Pr_{\mathrm{ave}}^{0.5}\left(\frac{\rho_{\mathrm{w}}}{\rho}\right)^{0.3} \tag{8}$$

$$Pr_{\mathrm{ave}} = Pr\frac{c_{\mathrm{p,ave}}}{c_{\mathrm{p}}} \tag{9}$$

$$c_{\mathrm{p,ave}} = \frac{h - h_{\mathrm{ave}}}{T - T_{\mathrm{w}}} \tag{10}$$

where h is specific enthalpy, in $\mathrm{J{\cdot}kg^{-1}}$.

2.3. Model Validation

The model was divided into several elements and the element independence verification was carried out as show in Table 1. The results showed that when the number of units was 100, the outlet temperature of the fluid basically remained unchanged. Therefore, 100 units were selected for subsequent calculation in order to save time and cost.

Table 1. The element independence verification.

Number of Elements	$T_{\mathrm{h,out}}$/K	$T_{\mathrm{c,out}}$/K
50	617.83	423.84
100	617.83	423.85
150	617.83	423.85
200	617.83	423.85
300	617.83	423.85
500	617.83	423.85

In this paper, the simulation results are compared with previous experimental results [29]. The results are shown in Table 2, and the difference between the simulation values and the experimental values is less than 4%; thus, the model can be considered reliable.

Table 2. Comparison between simulation results and experimental results.

Fluids	d/m	l/m	T_{in}/K	m_{in}/kg/s	T_{out}/K—EXP. [29]	T_{out}/K—Numerical	Deviation
Molten salt	0.02	1	623.95	0.86	615.45	617.83	0.39%
oil	0.034	1	425.35	0.465	425.35	423.84	0.36%

3. Result and Discussion

3.1. Thermodynamic Analysis under Constant Heat Transfer Area

The definitions of the entransy dissipation rate (ϕ_g), entransy dissipation number (N_{ED}), entransy dissipation thermal resistance (R_g), entropy production rate (S_g), and improve entropy production number (N_{RS}) are as follows:

$$\phi_g = \left(\frac{1}{2}C_h T_{h,in}^2 + \frac{1}{2}C_c T_{c,in}^2\right) - \left(\frac{1}{2}C_h T_{h,out}^2 + \frac{1}{2}C_c T_{c,out}^2\right) \tag{11}$$

where C is thermal capacity, in J/K.

$$N_{ED} = \frac{\left(\frac{1}{2}C_h T_{h,in}^2 + \frac{1}{2}C_c T_{c,in}^2\right) - \left(\frac{1}{2}C_h T_{h,out}^2 + \frac{1}{2}C_c T_{c,out}^2\right)}{Q(T_{h,in} - T_{c,in})} \tag{12}$$

where the heat flow Q is calculated as

$$Q = mc_p\Delta T \tag{13}$$

$$R_g = \left[\left(\frac{1}{2}C_h T_{h,in}^2 + \frac{1}{2}C_c T_{c,in}^2\right) - \left(\frac{1}{2}C_h T_{h,out}^2 + \frac{1}{2}C_c T_{c,out}^2\right)\right]/Q^2 \tag{14}$$

$$S_g = C_h \ln\frac{T_{h,out}}{T_{h,in}} + C_c \ln\frac{T_{c,out}}{T_{c,in}} \tag{15}$$

$$N_{RS} = T_{c,in}\left[C_h \ln\frac{T_{h,out}}{T_{h,in}} + C_c \ln\frac{T_{c,out}}{T_{c,in}}\right]/Q \tag{16}$$

The influence of the inlet temperature/inlet mass flow rate of molten salt and sCO_2 on the above parameters are analyzed below.

3.1.1. The Effect of Inlet Temperature and Inlet Mass Flow Rate of Molten Salt

Firstly, the effects of the inlet temperature and inlet mass flow rate of molten salt are studied. Figure 3 shows the variation in ϕ_g, N_{ED}, R_g, S_g, and N_{RS} versus the inlet temperature of molten salt.

As can be seen from Figure 3a,d, when the inlet mass flow rate of molten salt is the same, ϕ_g and S_g increase with the increase in the inlet temperature. This is because the increasing of molten salt temperature increases the heat exchange temperature difference between the two working medium, and as irreversible loss increases, ϕ_g will increase. Furthermore, ϕ_g and S_g increase as the mass flow rate increases, and when the mass flow rate increases, the heat transfer is intensified, making it easier to achieve heat transfer, and therefore the irreversible loss increases. In Figure 3b, the N_{ED} decreases as the temperature of the molten salt inlet increases, as $\phi_{g,max}$ increases more than ϕ_g as the temperature of the molten salt inlet increases. When the inlet temperature is the same, N_{ED} increases with the increase in mass flow rate, which is mainly caused by a larger increase in ϕ_g than $\phi_{g,max}$. In Figure 3c, at the same mass flow rate of molten salt, R_g decreases with the increase in inlet temperature, and when the inlet temperature is the same, R_g decreases with the increase in mass flow rate, which is the result of the different growth rates of Q and ϕ_g.

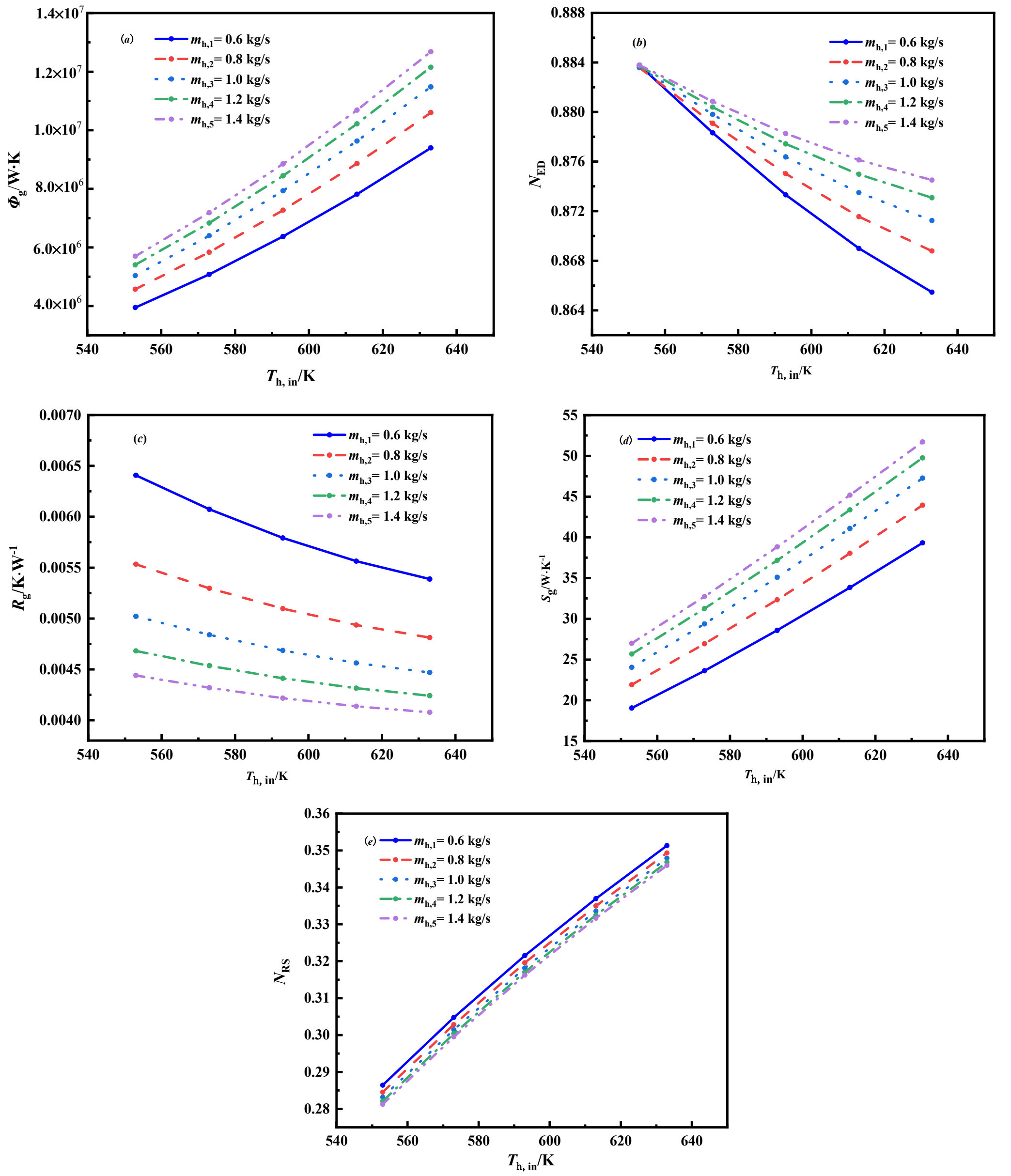

Figure 3. The ϕ_g (**a**), N_{ED} (**b**), R_g (**c**), S_g (**d**), and N_{RS} (**e**) versus the inlet temperature of molten salt.

In Figure 3e, it can be seen that N_{RS} increases with the increase in inlet temperature, because S_g and Q both increase with the increase in inlet temperature, but S_g has a larger increase than Q. At the same inlet temperature, N_{RS} decreases with the increase in mass flow rate, which is caused by the larger increase in Q than S_g.

3.1.2. The Effect of Inlet Temperature of sCO_2

Figure 4 shows the variations in ϕ_g, N_{ED}, R_g, S_g, and N_{RS} in the heat exchanger with the inlet temperature of sCO_2. As can be seen from Figure 4a,d, ϕ_g and S_g decrease with the increase in the inlet temperature of sCO_2, because the increase in the inlet temperature of sCO_2 reduces the heat transfer temperature difference between the two working media and the irreversible loss. When the inlet temperature of sCO_2 remains unchanged, ϕ_g and S_g increase with the increase in the inlet temperature of molten salt, which is also caused by the increase in the heat exchange temperature difference between the two working fluids and the increase in irreversible loss. As show in Figure 4b,c, N_{ED} and R_{g} decrease with the increase in the inlet temperature of sCO_2. This is because, as the inlet temperature of sCO_2 increases, the values of ϕ_{g} and $\phi_{\mathrm{g,max}}$ decrease, but ϕ_{g} decreases more than $\phi_{\mathrm{g,max}}$; therefore, the values of N_{ED} and R_{g} decrease. When the inlet temperature of sCO_2 remains unchanged, N_{ED} and R_{g} decrease with the increase in molten salt inlet temperature, and the temperature difference between the two fluids increases, so that ϕ_{g} and $\phi_{\mathrm{g,max}}$ both increase, but $\phi_{\mathrm{g,max}}$ is larger than ϕ_{g}; therefore, N_{ED} and R_{g} will decrease accordingly. In Figure 4e, N_{RS} decreases with the increase in the inlet temperature of sCO_2, because with the increase in the sCO_2 inlet temperature, both S_{g} and Q decrease, but the value of S_{g} decreases more than Q; therefore, N_{RS} will decrease accordingly. When the inlet temperature of sCO_2 remains unchanged, N_{RS} increases with the increase in molten salt inlet temperature, because with the increase in the molten salt inlet temperature, both S_{g} and Q increase, but S_{g} increases more than Q; therefore, the value of N_{RS} will increase accordingly.

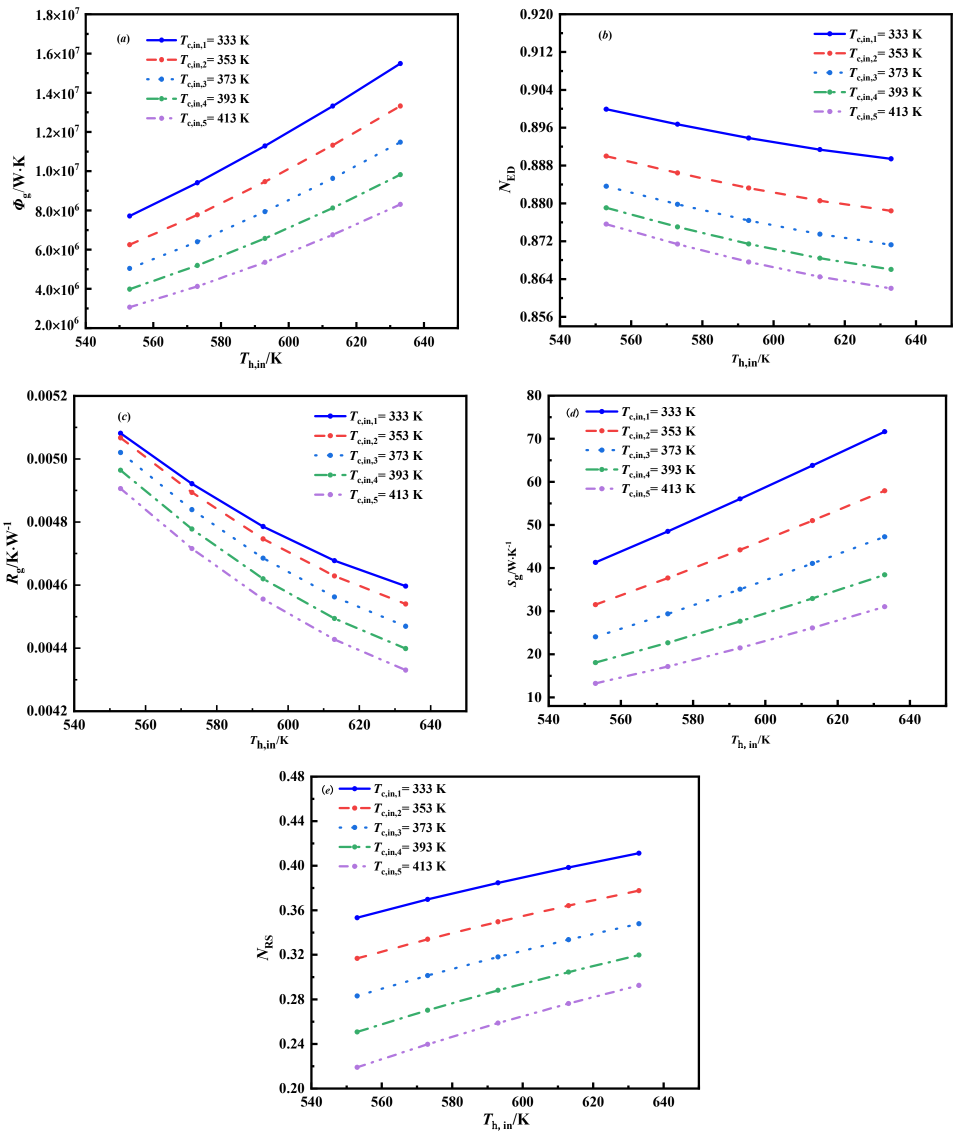

Figure 4. The ϕ_{g} (**a**), N_{ED} (**b**), R_{g} (**c**), S_{g} (**d**), and N_{RS} (**e**) versus the inlet temperature of sCO_2.

3.1.3. The Effect of Inlet Mass Flow Rate of sCO_2

Figure 5 shows the variation in ϕ_{g}, N_{ED}, R_{g}, S_{g}, and N_{RS} in the heat exchanger with the inlet mass flow rate of sCO_2. The variation trend of the above five parameters with the inlet mass flow rate of sCO_2 has many similarities with the variation trend of the inlet mass flow rate of molten salt in Section 3.1.1, and two differences will be explained here. The one is N_{ED}, which shows the opposite trend in the two cases; that is, in Section 3.1.1, the calculation points are concentrated first and then scattered. Here, however, the calculation points are first scattered and then concentrated. The other difference is N_{RS}, also showing the opposite trend in the two cases; that is, in Section 3.1.1, the molten salt inlet temperature is unchanged, and N_{RS} decreases with the increase of molten salt mass flow rate. However, the inlet temperature of sCO_2 remains unchanged, and N_{RS} increases with the increase in mass flow rate of sCO_2. This may be caused by the inconsistent effect of molten salt and sCO_2 on enhancing heat transfer by increasing the inlet mass flow rate; the changes in irreversible losses are also inconsistent.

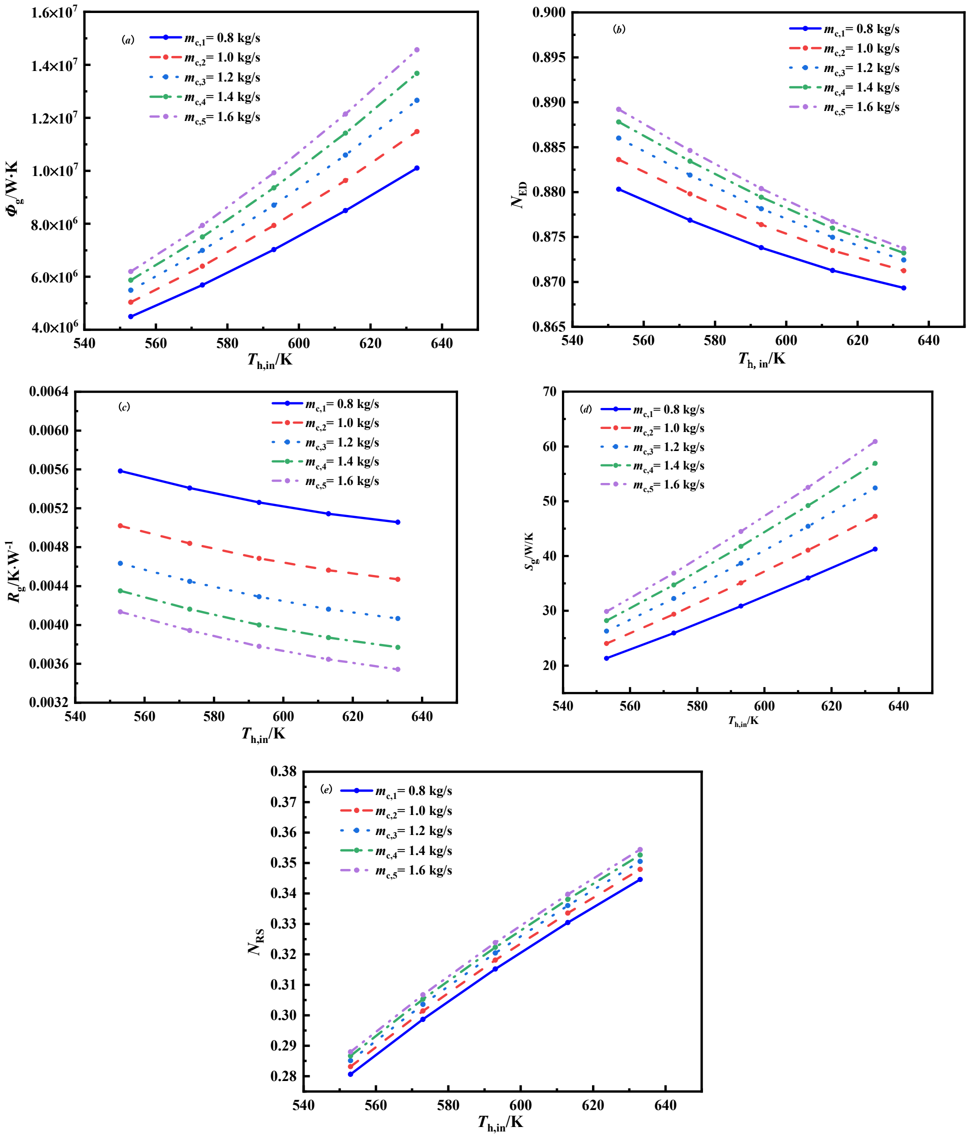

Figure 5. The ϕ_g (**a**), N_{ED} (**b**), R_g (**c**), S_g (**d**), and N_{RS} (**e**) versus the inlet mass flow rate of sCO_2.

3.2. Thermodynamic Analysis under Constant Heat Flux

Constant heat flux means that the heat flux in the heat exchange process remains unchanged; the inlet and outlet temperatures and mass flow rates of the molten salt also remained unchanged, which were 613 K, 603 K, and 1 kgs^{-1}, respectively.

3.2.1. The Effect of the Length of the Tube

Figure 6 shows the variation in ϕ_g, N_{ED}, R_g, S_g, and N_{RS} in the heat exchanger with the length of the tube. It can be seen from Figure 6a,c,e that ϕ_g , R_g, and N_{RS} decrease with the increase in the sCO_2 inlet temperature when the tube length is constant. When the sCO_2 inlet temperature is constant, ϕ_g, R_g, and N_{RS} decrease with the increase in tube length. The shorter the tube length, the smaller the resistance in the tube. If the same heat flux is still to be maintained, the mass flow of sCO_2 needs to be increased, resulting in enhanced heat transfer. The longer the tube length, the greater the resistance in the tube, and the more sufficient the heat exchange; therefore, it is not necessary to increase the mass flow of sCO_2 to maintain the same heat flux. As a result, heat transfer is enhanced, irreversible losses increase, and ϕ_g, R_g, and N_{RS} also increase. It can be seen from Figure 6b,d that the tube length is constant, and N_{ED} and S_g decrease with the increase in the inlet temperature of sCO_2. As the inlet temperature of CO_2 increases, ϕ_g and $\phi_{g,max}$ decrease at the same time, but ϕ_g decreases more than $\phi_{g,max}$; therefore, N_{ED} and S_g will decrease accordingly. At the same inlet temperature of sCO_2, N_{ED} decreases with increasing tube length. At the same inlet temperature of sCO_2, ϕ_g decreases with increasing tube length, so N_{ED} and S_g decrease accordingly.

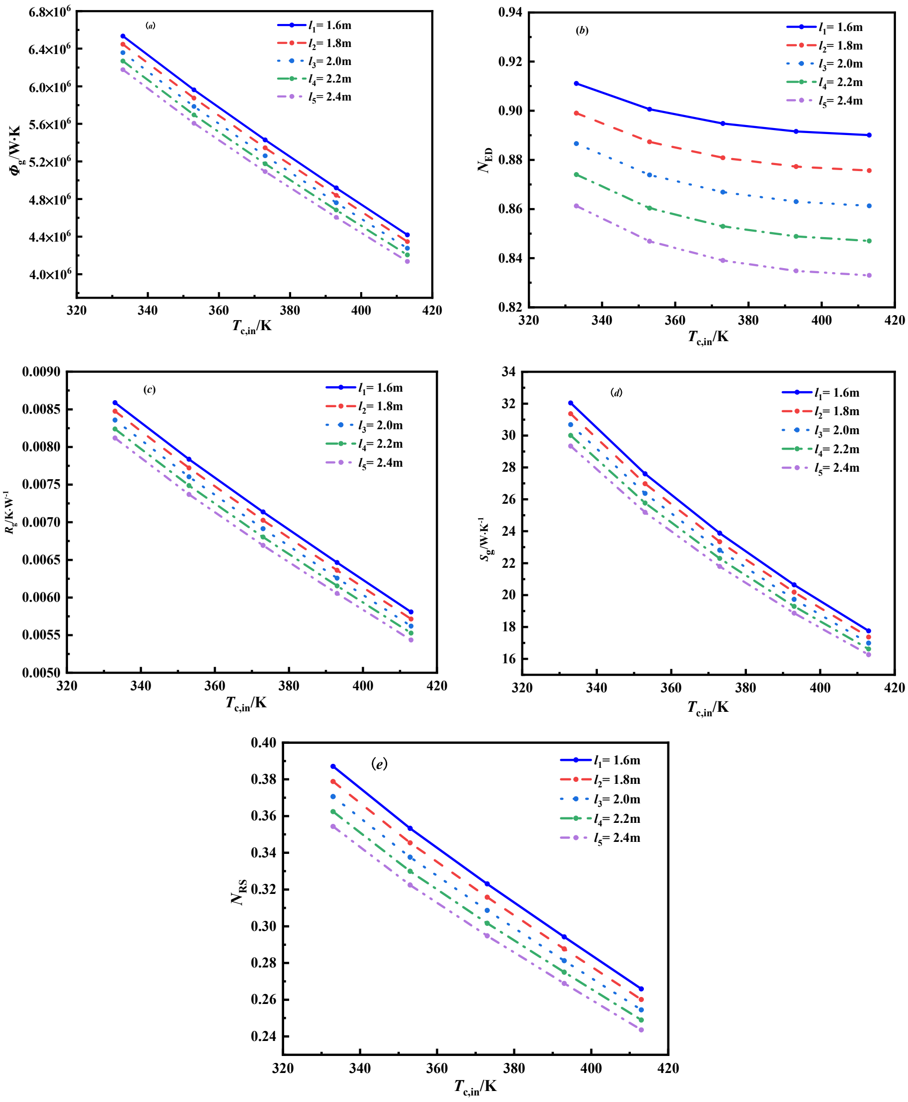

Figure 6. The ϕ_g (**a**), N_{ED} (**b**), R_g (**c**), S_g (**d**), and N_{RS} (**e**) versus the length of the tube.

3.2.2. The Effect of the Inner Diameter

Figure 7 shows the variations in ϕ_g, N_{ED}, R_g, S_g, and N_{RS} in the heat exchanger with the inner diameter. In Figure 7a,c–e, when the inner diameter is the same, ϕ_g, R_g, S_g, and N_{RS} decrease with the increase of sCO_2 inlet temperature. When the molten salt inlet parameters remain unchanged, the increase in the sCO_2 inlet temperature reduces the heat transfer temperature difference between the two working fluids and the irreversible loss, and ϕ_g, R_g, S_g, and N_{RS} will decrease accordingly. At the same sCO_2 inlet temperature, ϕ_g, R_g, S_g, and N_{RS} decreases with the increase in inner diameter, the heat transfer area on the molten salt side increases with the increase in inner diameter, the heat transfer of the molten salt weakens when the mass flow rate of the molten salt remains unchanged, and the irreversible loss decreases; therefore, ϕ_g, R_g, S_g, and N_{RS} will decrease accordingly. It can be seen from Figure 7b that when the inner diameter is the same, N_{ED} first decreases and then increases with the increase in sCO_2 inlet temperature. As the inlet temperature of sCO_2 increases, both ϕ_g and $\phi_{g,max}$ decrease, but there is an optimal sCO_2 inlet temperature that makes the ratio of ϕ_g and $\phi_{g,max}$ reach an extreme value. At the same sCO_2 inlet temperature, N_{ED} decreases with the increase in inner diameter, the heat exchange area on the molten salt side increases when the inner diameter increases, and, when the mass flow on the molten salt side remains unchanged, the heat transfer on the molten salt side weakens. Both ϕ_g and $\phi_{g,max}$ decrease, but ϕ_g decreases more than $\phi_{g,max}$; therefore, N_{ED} decreases accordingly.

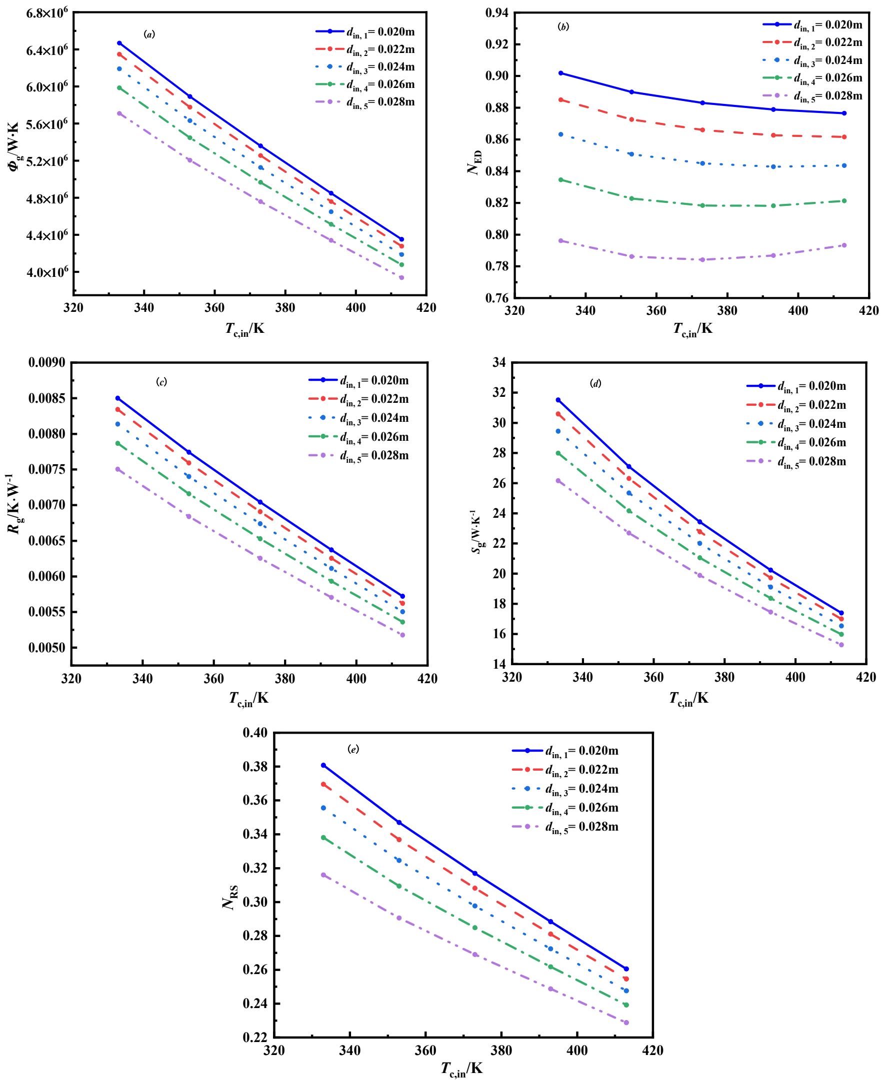

Figure 7. The ϕ_g (**a**), N_{ED} (**b**), R_g (**c**), S_g (**d**), and N_{RS} (**e**) versus the inner diameter.

3.2.3. The Effect of Outer Diameter

Figure 8 shows the variation in ϕ_g, N_{ED}, R_g, S_g, and N_{RS} in the heat exchanger with the outer diameter. At the same sCO_2 inlet temperature, ϕ_g, N_{ED}, R_g, S_g, and N_{RS} increase with the increase in outer diameter, the heat transfer area on the sCO_2 side increases with the increase in outer diameter, and the heat transfer of the sCO_2 weakens when the mass flow rate of the sCO_2 remains unchanged, and the irreversible loss increases; therefore, ϕ_g, N_{ED}, R_g, S_g, and N_{RS} will increase accordingly.

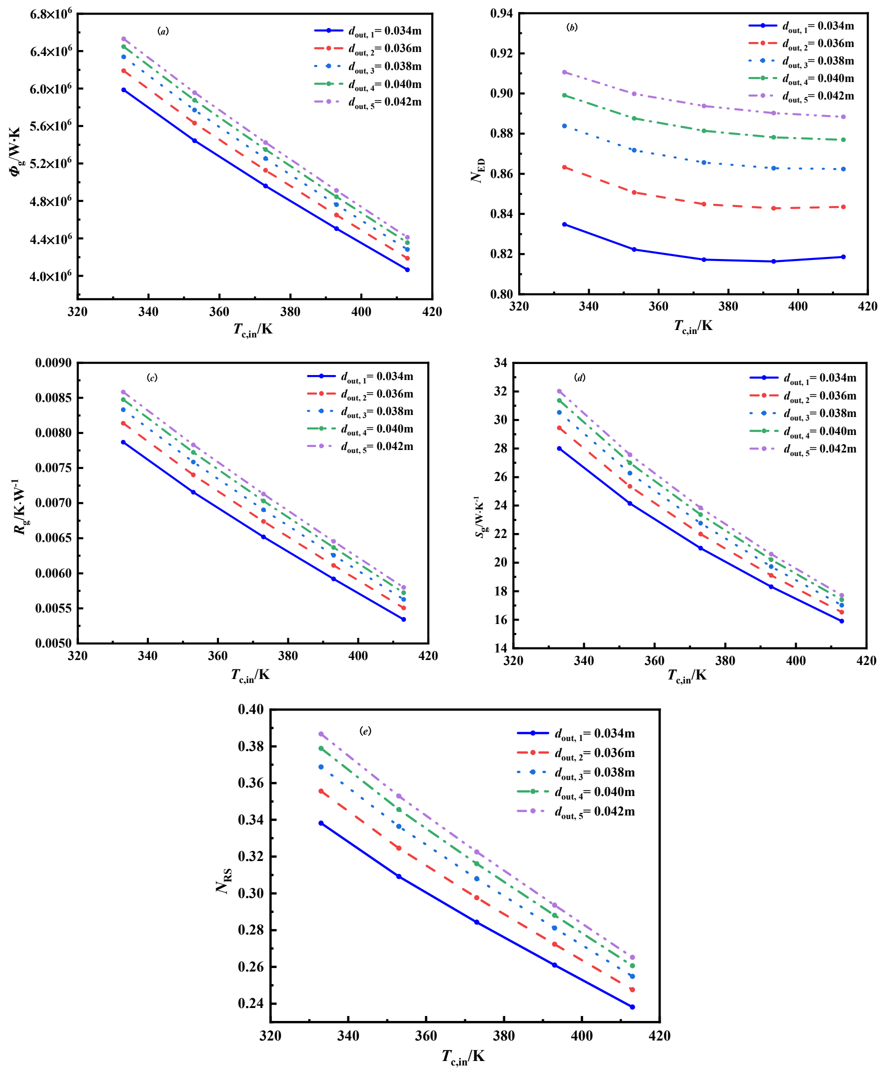

Figure 8. The ϕ_g (**a**), N_{ED} (**b**), R_g (**c**), S_g (**d**), and N_{RS} (**e**) versus the outer diameter.

3.3. Optimization Analysis of the Concentric Tube Heat Exchanger

In this part, the geometric and operating parameters of the heat exchanger will be optimized and analyzed, and the optimized variables and ranges are shown in Table 3.

Table 3. Optimized parameters and ranges.

Parameters	Ranges	Parameters	Ranges
d_{in}/m	0.015–0.035	d_{out}/m	0.030–0.050
l/m	1.6–2.4	$T_{h,in}$/K	543.15–583.15
$T_{c,in}$/K	323.15–363.15	m_h/kg/s	0.8–1.0
m_c/kg/s	1.0–1.2		

3.3.1. Single-Objective Optimization Analysis

The objective functions of the single-objective optimization calculation of the heat exchanger were measured using the following: ϕ_g, N_{ED}, R_g, S_g, N_{RS}, Q, the pressure entransy dissipation number (N_P), the total heat transfer coefficient (α), and heat transfer effectiveness (ε). The expression of N_P, h, and ε are shown in Equations (17)–(19).

$$N_P = \frac{\frac{m_h \Delta P_h}{\rho_h} \frac{T_{h,out} - T_{h,in}}{\ln T_{h,out} - \ln T_{h,in}} + \frac{m_c \Delta P_c}{\rho_c} \frac{T_{c,out} - T_{c,in}}{\ln T_{c,out} - \ln T_{c,in}}}{Q(T_{h,in} - T_{c,in})} \quad (17)$$

$$\alpha = \frac{Q}{F \Delta T_m} \quad (18)$$

where ΔT_m is the logarithmic mean temperature difference, in K.

$$\varepsilon = \frac{\max((T_{h,in} - T_{h,out}), (T_{c,out} - T_{c,in}))}{T_{h,in} - T_{c,in}} \quad (19)$$

It will be discussed in two aspects: on the one hand, the corresponding results of each objective function are obtained; on the other hand, the values of other objective functions are calculated according to the optimization results of a certain objective function. The optimization results are shown in Table 4.

Table 4. Single-objective optimization calculation results.

	Single Objective Optimization Objective Function									
	Ref	**min(ϕ_g)**	**min(N_{ED})**	**min(R_g)**	**min(S_g)**	**min(N_{RS})**	**min(N_P)**	**max(α)**	**max(Q)**	**max(ε)**
d_{in}/m	0.02	0.015	0.017	0.018	0.015	0.02	0.022	0.015	0.015	0.017
d_{out}/m	0.034	0.05	0.031	0.032	0.05	0.034	0.05	0.03	0.03	0.031
l/m	2	1.6	2.4	2.397	1.6	2.4	1.647	1.609	2.4	2.4
$T_{h,in}$/K	563.15	543.15	583.14	583.12	543.15	543.15	574.31	583.13	583.15	583.15
$T_{c,in}$/K	343.15	346.15	363.15	363.14	363.15	363.15	323.25	363.14	323.15	363.15
m_h/kg/s	0.8	0.8	0.8	0.999	0.8	0.998	0.839	1	1	1
m_c kg/s	1.2	1	1	1.199	1	1.001	1.024	1.2	1.2	1.001
ϕ_g	7,491,097	1,798,047	8,245,213	9,817,459	1,798,047	5,624,994	4,919,799	7,083,193	14,124,153	8,985,178
N_{ED}	0.891	0.957	0.849	0.854	0.957	0.862	0.957	0.901	0.891	0.850
S_g	0.00513	0.01651	0.00423	0.00359	0.01651	0.00428	0.01174	0.00554	0.00380	0.00390
R_g	38.496	9.074	38.136	45.376	9.074	27.960	26.484	32.950	74.511	41.263
N_{RS}	0.346	0.316	0.314	0.315	0.316	0.280	0.418	0.335	0.395	0.312
N_P	9.17×10^{-6}	3.08×10^{-6}	1.14×10^{-5}	1.49×10^{-5}	3.08×10^{-6}	1.24×10^{-5}	4.64×10^{-7}	1.44×10^{-5}	5.98×10^{-6}	1.13×10^{-5}
h	1563.287	804.2732	1867.839	2079.548	804.2732	1565.425	749.1298	2391.515	2207.722	2027.949
Q/W	38,213.33	10,437.41	44,146.8	52,291.34	10,437.41	36,248.61	20,467.84	35,746.22	60,983.57	48,021.55
ε	0.119	0.046	0.168	0.166	0.046	0.167	0.053	0.112	0.128	0.183

It can be seen from Table 4 that when the single-objective optimization calculation of the heat exchanger is performed for each objective function, each objective function corresponding to the variable range can obtain its own extreme value, but the corresponding other objective function values are not optimal. It shows that single-objective optimization has strong pertinence. In addition, if the heat exchange effectiveness (ε) is used as the evaluation index of the performance of the heat exchanger, the minimum ϕ_g and S_g are taken as the objective functions, meaning the heat exchange effectiveness is low and the effect is poor. However, with the N_{ED}, R_g, and N_{RS} minimums as objective functions, a better optimization effect can be obtained, where the ε value is increased by 41.2%, 39.5%, and 40.3% compared with the reference individual.

3.3.2. Multi-Objective Optimization Analysis

The single-objective optimization results can ensure that the selected objective function obtains the extreme value; however, it cannot guarantee that the other performance parameters of the heat exchanger are ideal, which indicates that there is an opposite relationship between the objective functions. Since these objective functions can reflect certain aspects of the performance of a heat exchanger, the performance of some aspects of the heat exchanger can be improved, whereas the performance of other aspects will be suppressed. Different from single-objective optimization, the advantage of multi-objective optimization is that it can optimize the heat exchanger from multiple angles, so that each objective function in multi-objective optimization can obtain extreme values.

It can be seen from the single-objective optimization results that the optimization effect is better with the N_{ED}, R_g, and N_{RS} minimums and ε maximum as the objective function;

so, it was adopted in the multi-objective optimization. N_P reflects the irreversible loss of the heat exchanger due to the flow resistance of the working medium. Therefore, the following multi-objective function combination was selected to optimize the casing heat exchanger, N_{ED} and N_P minimum, R_g and N_P minimum, N_{RS} and N_P minimum, ε maximum, and N_P minimum. The multi-objective optimization calculation results are shown in Table 5.

Table 5. Multi-objective optimization calculation results.

	Single-Objective Optimization Objective Function					**Multi-Objective Optimization Objective Function**			
	Ref	**min(N_{ED})**	**min(R_g)**	**min(N_{RS})**	**max(ε)**	**min(N_{ED}) + min(N_P)**	**min(R_g) + min(N_P)**	**min(N_{RS}) + min(N_P)**	**max(ε) + min(N_P)**
d_{in}/m	0.02	0.017	0.018	0.02	0.017	0.0213	0.0285	0.0255	0.0208
d_{out}/m	0.034	0.031	0.032	0.034	0.031	0.035	0.043	0.040	0.035
l/m	2	2.4	2.397	2.4	2.4	2.398	2.392	2.397	2.361
$T_{h,in}$/K	563.15	583.14	583.11	543.152	583.15	547.17	566.59	543.21	566.39
$T_{c,in}$/K	343.15	363.15	363.14	363.14	363.15	344.65	324.149	363.15	323.60
m_h kg/s	0.8	0.8	0.999	0.998	1	0.993	1	0.894	0.820
m_c kg/s	1.2	1	1.199	1.001	1.001	1.021	1.171	1.016	1.182
ϕ_g	7,491,097	8,245,213	9,817,459	5,624,994	8,985,178	7,188,210	10,923,844	5,113,361	10,479,204
N_{ED}	0.891	0.849	0.854	0.862	0.850	0.875	0.903	0.872	0.896
S_g	0.00513	0.004231	0.00359	0.004281	0.003896	0.004366	0.004389	0.004818	0.004516
R_g	38.496	38.136	45.376	27.960	41.263	37.443	59.197	25.524	57.252
N_{RS}	0.345692	0.314	0.315	0.280	0.312	0.318	0.385	0.285	0.385
N_P	9.17×10^{-6}	1.14×10^{-5}	1.49×10^{-5}	1.24×10^{-5}	1.13×10^{-5}	7.28×10^{-6}	2.74×10^{-6}	9.34×10^{-6}	4.27×10^{-6}
α	1563.287	1867.839	2079.548	1565.425	2027.949	1441.761	1071.811	1091.082	1449.806
Q/W	38,213.33	44,146.8	52,291.34	36,248.61	48,021.55	40,577.45	49,887.39	32,577.88	48,170.41
ε	0.119	0.168	0.166	0.1676	0.1836	0.146	0.113	0.147	0.133
ΔP_h	5.017	12.580	37.607	9.212	28.091	6.689	1.628	2.414	5.163
ΔP_c	28.911	14.084	48.759	18.516	38.893	24.539	16.155	19.511	24.305

The corresponding multi-objective optimization calculation results were compared with the single-objective optimization calculation results, and the heat transfer effectiveness and pressure drop were used as indicators to evaluate the optimization calculation results. Compared with the reference, the heat exchange efficiency corresponding to the single-objective optimization results with the N_{ED}, R_g and N_{RS} minimum and ε maximum as the objective functions have been improved to varying degrees, but the pressure drop of the working fluid has also increased, indicating that the improvement in heat transfer efficiency is achieved at the expense of an increasing pressure drop. Compared with the reference and single-objective optimization calculation results, the heat transfer efficiency of the multi-objective optimization calculation results is not as large as that of the single-objective optimization calculation results, and even the heat exchange efficiency is lower than that of the reference individual; but, the pressure drop in the tube is more obvious, which shows the opposite nature of each objective function in multi-objective optimization and the result of balancing the objective function. In addition, the comprehensive effect of the multi-objective optimization calculation results with the N_{RS} and N_P minimums as the objective function is optimal. Compared with the reference individual, the ε value increased by 23.5%, and ΔP_h and ΔP_c decreased by 51.9%, and 32.5%, respectively.

4. Conclusions

This paper takes a concentric tube heat exchanger as the research object, with molten salt and sCO_2 used as the heat transfer medium, and performed thermodynamic and optimization calculations.

On the one hand, the thermodynamic analysis was carried out, by using the distributed parameter method, to model the heat exchanger and the effects of the structural parameters and operating parameters of the heat exchanger on the entransy dissipation rate, the entransy dissipation number, the entransy dissipation thermal resistance, entropy production rate and entropy production number. The results show that the structural parameters and operating parameters of the heat exchanger have different effects on the entropy dissipation, the entropy dissipation number, the entropy dissipation thermal resistance, the entropy production rate, and the entropy production number. Furthermore, the entransy dissipation rate and entropy production rate showed the same trend in structural parameters and operating parameters, and the changes in the entransy dissipation number and entransy dissipation thermal resistance were jointly affected by the entransy dissipation rate and the heat exchange.

On the other hand, single-objective and multi-objective optimizations were carried out, and it was found that single-objective optimization had strong pertinence, and the optimization results could only greatly improve the performance of a certain aspect of the heat exchanger. Taking the N_{ED}, R_{g}, and N_{RS} minimums as the objective functions, the heat transfer efficiency was high, and the optimization effect was better. The ε values increased by 41.2%, 39.5%, and 40.3% compared with the reference individual. Multi-objective optimization can improve the limitations of single-objective optimization. From the perspective of improving comprehensive performance, the heat exchanger was optimized to keep the performance of the heat exchanger in balance. The multi-objective optimization calculation results with the N_{RS} and N_{P} minimums as the objective functions have more comprehensive, better results. Compared with the reference individual, the ε value increased by 23.5%, and ΔP_{h} and ΔP_{c} decreased by 51.9% and 32.5%, respectively.

Author Contributions: Methodology, Y.W., Y.L. and C.M.; Writing—original draft, X.D.; Writing—review & editing, C.Z. All authors have read and agreed to the published version of the manuscript.

Funding: This research was funded by [National Natural Science Foundation of China] grant number [51906003], [Science and technology general project of Beijing Municipal Education Commission] grant number [KM202210005016] and [the Inner Mongolia Science and Technology Major Project] grant number [2021ZD0036].

Data Availability Statement: The data used to support the findings of this study are available from the corresponding author upon request.

Conflicts of Interest: The authors declare no conflict of interest.

Nomenclature

A	cross-sectional area, m^2	C	thermal capacity, J·K^{-1}
c_{p}	specific heat capacity, J·kg^{-1}·K^{-1}	d_{in}	inner diameter, m
d_{out}	outer diameter, m	D	equivalent diameter, m
F	total heat exchange area, m^2	f	the resistance coefficient
h	specific enthalpy, J·kg^{-1}	l	the length of heat exchanger, m
m	mass flow rate, kg·s^{-1}	Nu	Nusselt number
N_{ED}	entransy dissipation number	N_{RS}	improve entropy production number
N_{p}	pressure entransy dissipation number	P	pressure, Pa
ΔP	pressure drop, Pa	Pr	Prandlt number
Q	heat transfer rate, W	Re	Reynold number
R_{g}	entransy dissipation thermal resistance, K·W^{-1}	S_{g}	entropy production rate, W·K^{-1}
sCO_2	supercritical CO_2	T	temperature, K
ΔT	temperature difference, K	ΔT_{m}	logarithmic mean temperature difference, K
u	velocity, m·s^{-1}	x	x-direction component, m
Greek symbols			
α	heat transfer coefficient, W·m^{-2}·K^{-1}	ε	heat transfer effectiveness
λ	thermal conductivity, W·m^{-1}·K^{-1}	μ	dynamic viscosity, kg·m^{-1}·s^{-1}
ρ	density, kg·m^{-3}	ϕ_{g}	entransy dissipation rate, W·K
Subscript			
ave	average	c	cold
h	hot	in	inside
max	maximum	out	outside
w	wall		

References

1. Mehos, M.; Turchi, C.; Vidal, J. *Concentrating Solar Power Gen 3 Demonstration Roadmap*; Technical Report; NREL: Oslo, Norway, 2017.
2. Han, Y.; Zhang, C.C.; Wu, Y.T.; Lu, Y.W. Investigation on thermal performance of quaternary nitrate-nitrite mixed salt and solar salt under thermal shock condition. *Renw. Energyi.* **2022**, *175*, 1041–1051. [CrossRef]
3. Zhang, C.C.; Han, S.T.; Wu, Y.T.; Zhang, C.Y.; Guo, H. Investigation on convection heat transfer performance of quaternary mixed molten salt based nanofluids in smooth tube. *Int. J. Therm. Sci.* **2022**, *177*, 107534. [CrossRef]
4. Bhuvaneswari, S.; Elatharasan, G. A Study of the Literature Review on Heat Transfer in A Helically Coiled Heat Exchanger. *Int. J. Eng. Res. Technol.* **2019**, *7*, 1–3.
5. Mylavarapu, S.K.; Figley, J.; Sun, X.; Christensen, R.N.; Needler, N.J.; Hajek, B.K. Development and testing of printed circuit heat exchanger for generation IV reactors. *Trans. Am. Nucl. Soc.* **2008**, *98*, 626–627.
6. Bejan, A. Entropy Generation Minimization: The New Thermodynamics of Finite-Size Devices and Finite-Time Processes. *J. Appl. Phys.* **1996**, *79*, 1191–1218. [CrossRef]
7. Bejan, A. *Second-Law Analysis in Heat Transfer and Thermal Design*; Elsevier: New York, NY, USA, 1982; pp. 1–58.
8. Hesselgreaves, J.E. Rationalisation of second law analysis of heat exchangers. *Int. J. Heat Mass Transf.* **2000**, *43*, 4189–4204. [CrossRef]
9. Ogiso, K. Duality of heat exchanger performance in balanced counter-flow systems. *J. Heat Transf.-Trans. AMSE* **2003**, *125*, 530–532. [CrossRef]
10. Shah, R.K.; Skiepko, T. Entropy generation extrema and their relationship with heat exchanger effectiveness-number of transfer unit behavior for complex flow arrangements. *J. Heat Transf.-Trans. AMSE* **2004**, *126*, 994–1002. [CrossRef]
11. Guo, Z.Y.; Zhu, H.Y.; Liang, X.G. Entransy: A Physical Quantity Describing Heat Transfer Ability. *Int. J. Heat Mass Transf.* **2007**, *50*, 2545–2556. [CrossRef]
12. Guo, F.; Cheng, L.; Xu, M.T. Entransy Dissipation Number and Its Application to Heat Exchanger Performance Evaluation. *Chin. Sci. Bull.* **2009**, *54*, 2998–3002. [CrossRef]
13. Lerou, P.P.P.M.; Veenstra, T.T.; Burger, J.F.; ter Brake, H.J.; Rogalla, H. Optimization of counterflow heat exchanger geometry through minimization of entropy generation. *Cryogenics* **2005**, *45*, 659–669. [CrossRef]
14. Chen, Q. Entransy dissipation-based thermal resistance method for heat exchanger performance design and optimization. *Int. J. Heat Mass Transf.* **2013**, *60*, 156–162. [CrossRef]
15. Wang, S.M.; Jian, G.P.; Sun, J.R. Application of entransy-dissipation-based thermal resistance for performance optimization of spiral-wound heat exchanger. *Int. J. Heat Mass Transf.* **2018**, *116*, 743–750. [CrossRef]
16. Guo, J.F.; Xu, M.T. The application of entransy dissipation theory in optimization design of heat exchanger. *Appl. Therm. Eng.* **2012**, *36*, 227–235. [CrossRef]
17. Qian, X.D.; Li, X.Z. Analysis of entransy dissipation in heat exchangers. *Int. J. Therm. Sci.* **2011**, *50*, 608–614. [CrossRef]
18. Cheng, X.T.; Zhang, Q.Z.; Liang, X.G. Analyses of entransy dissipation, entropy generation and entransy-dissipation-based thermal resistance on heat exchanger optimization. *Appl. Therm. Eng.* **2012**, *38*, 31–39. [CrossRef]
19. Liu, X.B.; Meng, J.A.; Guo, Z.Y. Entropy generation extremum and entransy dissipation extremum for heat exchanger optimization. *Chin. Sci. Bull.* **2009**, *54*, 943–947. [CrossRef]
20. Guo, J.F.; Xu, M.T.; Cheng, L. Principle of equipartition of entransy dissipation for heat exchanger design. *Sci China Tech Sci* **2010**, *53*, 1309–1314. [CrossRef]
21. Xie, G.N.; Song, Y.D.; Asadi, M.; Lorenzini, G. Optimization of Pin-Fins for a Heat Exchanger by Entropy Generation Minimization and Constructal Law. *J. Heat Transf. Trans. Asme* **2015**, *137*, 1–9. [CrossRef]
22. Guo, Z.Y.; Liu, X.B.; Tao, W.Q. Effectiveness–thermal resistance method for heat exchanger design and analysis. *International J. Heat Mass Transf.* **2010**, *53*, 2877–2884. [CrossRef]
23. Li, K.; Wen, J.; Liu, Y.C.; Liu, H.; Wang, S.; Tu, J. Application of entransy theory on structure optimization of serrated fin in plate-fin heat exchanger. *Appl. Therm. Eng.* **2020**, *173*, 114809. [CrossRef]
24. Han, Z.X.; Guo, J.F.; Huai, X.L. Research on optimization method of new airfoil heat exchanger based on entransy dissipation theory. *Chin. Sci. Technol. Sci.* **2021**, *51*, 1219–1230.
25. Han, Y.; Zhang, C.C.; Zhu, Y.J.; Wu, X.H.; Jin, T.X.; Li, J.N. Investigation of heat transfer Exergy loss number and its application in optimization for the shell and helically coiled tube heat exchanger. *Appl. Therm. Eng.* **2022**, *211*, 118424. [CrossRef]
26. Linstrom, P.J.; Mallard, W.G. National Institute of Standards and Technology: Gaithersburg, MD, USA, 2005, 2011. Available online: http://webbook.nist.gov/chemistry (accessed on 5 September 2022).
27. Gnielinski, V. New Equations for Heat and Mass Transfer in Turbulent Pipe and Channel Flows. *Int. J. Chem. Eng.* **1976**, *16*, 359–368.
28. Hall, W.B.; Jackson, J.D.; Watson, A. Forced convection heat transfer to fluids at supercritical pressure. In *Turbulent Forced Convection in Channels and Bundles*; Hemisphere: New York, NY, USA, 1979; Volume 2, pp. 563–611.
29. Chen, H.; Chen, X.; Wu, Y.T.; Lu, Y.W.; Wang, X.; Ma, C.F. Experimental study on forced convection heat transfer of KNO_3–$Ca(NO_3)_2$ + SiO_2 molten salt nanofluid in circular tube. *Sol. Energy* **2020**, *206*, 900–906. [CrossRef]